

## Solar Prominence Diagnostics

J.-C. Vial

*Institut d'Astrophysique Spatiale, CNRS/Université Paris XI, Bâtiment  
121, 91405 Orsay Cedex, France*

**Abstract.** This paper reviews the diagnostic techniques currently used to establish estimates of the physical properties of prominences. Most often the fine structure of prominences cannot be resolved. Because of this and the complex structures and the varied forms of prominences, it is difficult to establish definitive values for temperature, density, magnetic field, electric field, differential emission measure, mass flows, etc. Nevertheless, there are many useful techniques ranging from spectroscopic analysis to measurements of prominence oscillations. Most of the major techniques are reviewed in this paper, with examples of the results and an extensive bibliography. Special attention is paid to the potential diagnostic value of optically thick lines. Suggestions are made for further progress based on SOHO and other observations.

### 1. Introduction

For the last extensive review of this subject, we refer to the book "The Nature of Solar Prominences" by Tandberg-Hanssen (1995) (hereafter ETH), especially his Chapter 3. We want to stress three features from it:

- i. There is no such thing as a canonical prominence (see the different classifications in ETH).
- ii. No structure is really isolated (it has interfaces with the chromosphere and the corona).
- iii. No prominence has an uniform structure.

These three features have two consequences:

- i. A large range of values within a prominence and from prominence to prominence (which may also be due to the diagnostic techniques used).
- ii. The difficulty of the diagnostic, which is nevertheless necessary for building MHD models, in describing and explaining the formation and disappearance of prominences. We now describe the techniques commonly used to determine thermodynamic parameters.

### 2. Diagnostic of Thermodynamic Parameters

In order to understand the very existence of cool material in the corona, it is essential to precisely measure its temperature and the variation of temperature *within the structure, especially at the interface regions.*

## 2.1. Temperature

We refer here to the electron temperature since the density is sufficient to provide equal temperatures for the different species.

The first technique consists in the measurement of the profile shape of at least two lines of different elements which leads to the separation of temperature (5000–8000K) and associated “microturbulence” (5–8 km/s). See ETH and the Hvar Reference Model (Engvold et al. 1990). The above range of temperatures corresponds to the coolest material, although Hirayama et al. (1979) reported 4300K and 3 km/s for temperature and “microturbulence”, respectively. It must be noted that the technique assumes an optically thin plasma and neglects sources of broadening other than Doppler: pressure, electric fields, etc..

The color temperature of the Lyman continuum has been shown by Heasley and Milkey (1983) to represent the electron temperature, at least for layers that are not too thin. From Skylab observations, they derived values around 6500K. Higher temperatures exist in Active Region Prominences and, of course, in the Prominence Corona Transition Region (PCTR).

As for radio observations, the derived parameter is the brightness temperature,  $T_b$ . At  $l < 1$  cm,  $T_b$  of the cool material is 8000K; limb measurements performed with the JCMT (Harrison et al. 1993) indicate a *very* low temperature if a “reasonable” density is assumed. At  $l > 1$  cm (VLA observations),  $T_b$  of the PCTR goes up to 80,000K, a value which is much lower than the one deduced from EUV measurements (Engvold 1989). This disagreement has been discussed in terms of magnetic field orientation vs. height by Chiuderi-Drago et al. (1992) and could provide evidence of different PCTRs at the sides and top of filaments (see Chiuderi-Drago et al. 1998, these proceedings). We note that the Nobeyama telescope (17 GHz) has proven to be very useful for locating filaments and filament channels.

## 2.2. Densities

According to the Hvar Reference Atmosphere of Quiescent Prominences, the electron density is in the range  $10^{10} - 10^{11} \text{ cm}^{-3}$  in the cool part, down to  $10^8$  in the PCTR. This range is larger, because of the variety of methods used.

The most direct method (Stark effect in high Balmer lines) has been used recently by Hirayama (1990) who found about  $n_e \sim 10^{11} \text{ cm}^{-3}$ . On the other hand, line ratio techniques have been used in the visible (e.g., Na I to Sr II resonance lines ratio shown to be proportional to  $n_e$ ) by Landman (1985, 1986). They indicate that  $n_e$  is larger than  $10^{11} \text{ cm}^{-3}$ . Foukal et al. (1986) find  $n_e$  of the order of  $10^{11} \text{ cm}^{-3}$ . The line ratios technique in the infrared (Fe XIII 10747/10798Å) employed with the Pic-du-Midi Coronagraph provides evidence of a coronal cavity, although the density is not lower everywhere around the prominence (Wiik, Schmieder and Noens 1992). With the opportunity of an eclipse, Stellmacher, Koutchmy, and Lebecq (1986) measured the  $H\beta$  line to continuum ratio and derived a density of about  $3 \times 10^9 \text{ cm}^{-3}$ . In the UV, line ratios such as O IV (1401/1404Å) lead to  $n_e \sim 10^{11} \text{ cm}^{-3}$  (Wiik et al. 1993).

An interesting by-product of the work on the Hanle effect consists in measurement of the depolarization in two lines, one, such as  $D_3$ , being depolarized by the magnetic field only, the other, such as  $H\beta$  or  $H\alpha$ , depolarized by both magnetic field and collisions. In this way, the effect of collisions can be evaluated

and the electron density derived. Bommier et al. (1986, 1994) found  $n_e$  in the range  $3 \times 10^9 - 4 \times 10^{10} \text{ cm}^{-3}$ .

Radio prominence measurements performed in the mm range with the VLA (Bastian et al. 1993) and the JCMT (Harrison et al. 1993) also point to low values (about  $10^{10} \text{ cm}^{-3}$ ). Of course, the very existence of such low densities implies large effective thicknesses, as noted by Hirayama (1990).

### 2.3. Ionization Degree (ID)

As shown by Poland et al. (1971), the cool parts of prominences are ionized by the H and He Lyman incident radiation. The ionization degree (ID) is a crucial parameter for the determination of pressure, flows, and balance of forces (mass to current ratio). Here, we define ID by the ratio of proton density to neutral hydrogen density. It is roughly equal to the ratio of electron density (the helium ionization is reduced) to the density of the level 1 population  $n_e/n_1$ . In the Hvar Reference Atmosphere, the ionization is described by the ratio X of electron density to the **total** hydrogen density. Between the two quantities, we have the relation:  $ID = 1/(X^{-1} - 1)$ . Assuming we know  $n_e$  we must determine  $n_1$ . There is no direct technique: the idea is to determine the opacity at the head of the  $L_\infty$ : Landman (1983, 1984) found  $ID \ll 1$ . According to ETH, "the best range of values for quiescent prominences is probably:  $0.05 < ID < 1$ ". In a loop prominence, Heinzel and Vial (1992) found  $ID = 0.9$ . Measuring obscuration effects in the EUV (Skylab), Schmahel and Orrall (1979, 1986) derived larger IDs in the range 2–10. Let's also mention that by deriving a proportionality between the ratio of intensities  $L\alpha/\text{CaK}$  and  $ID^2$ , Vial (1982) could bracket, from OSO8 observations, the ID between 1 and 10.

The NLTE modelling of Gouttebroze et al. (GHV 1993) and Heinzel et al. (HGV 1994) lead to an ID of about 10 for low densities (Figure 1). As shown by Figure 1, the ionization (measured here by the X parameter) does not change much with temperature as long as the densities are low. This reflects the domination of radiation in the ionization process.

With the large range of values of ID goes a large range of gas pressures with  $P_g$  (cgs)  $\sim 0.1$ – $1$  (0.02 at the edges). Let's say that the NLTE models (discussed in Section 3) favor low pressure values. From the He singlet/triplet, Stellmacher and Wiehr (1997) could measure the total hydrogen density ( $3 \times 10^{10} \text{ cm}^{-3}$ ) and conclude that the pressure P is about  $0.02 \text{ dyn cm}^{-2}$ .

### 2.4. Differential Emission Measure (DEM) in the PCTR

The DEM as defined by  $n_e^2 (dT/dz)^{-1}$  is similar in the PCTR to the DEM in the CCTR. This shape is well explained at temperatures higher than  $10^5 \text{ K}$  where radiative losses balance conduction energy gain. But for temperatures lower than  $10^5 \text{ K}$ , no real explanation has been provided. Engvold (1989) refers to flows and enthalpy flux. Rabin (1986) proposes perpendicular conductivity which can only work if many thin layers constitute the PCTR. Chiuderi and Chiuderi-Drago (1991) and Chiuderi-Drago et al. (1992) studied the effect of a large angle between the temperature gradient and the magnetic field vector and its effect on the perpendicular conductivity. Still, an extra energy input is needed at low T which could be the dissipation of Alfvén waves (see also Chiuderi-Drago et al. 1998, these proceedings).

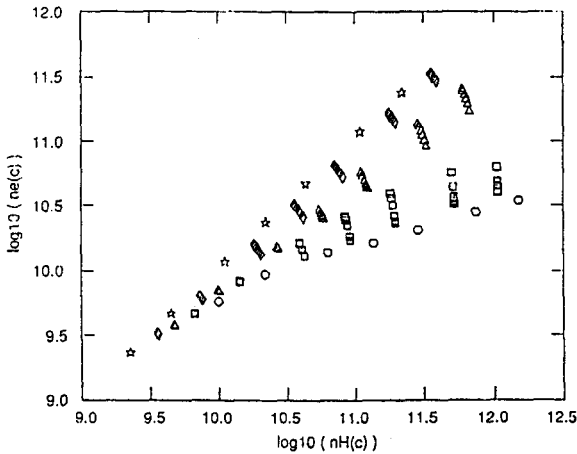


Figure 1. Logarithmic plot of the variation of electron density with total hydrogen density at the center of different slabs with different pressures, widths and temperatures ranging from 4300 K (circles) to 15,000K (stars). From HGV.

## 2.5. Velocities (Flows)

We must distinguish between the cases of quiescent and active prominences. In quiescent prominences, both upward and downward vertical motions have been found (see Schmieder 1990 and ETH). *Downflows* of about  $0.5 \text{ km s}^{-1}$  have been observed both at the limb (apparent motions) and on the disk (Doppler). *Upflows*, usually less than  $5 \text{ km s}^{-1}$ , have been observed on the disk (Doppler), e.g., above filament feet. As for horizontal motions (only measured at the limb with the Doppler technique), values of about  $10\text{--}20 \text{ km s}^{-1}$  can be found at all temperatures (up to  $60 \text{ km s}^{-1}$  in active region prominences), especially at the edges. This leads to the rather surprising result that horizontal velocities are seemingly larger than vertical ones. However, from systematic limb-to-limb measurements performed in the C IV line observed with UVSP/SMM, Simon et al (1986) showed that at  $10^5 \text{ K}$ , vertical velocities are larger than horizontal ones. They interpret these results as flows occurring within small loops. The non-visibility of vertical velocities at temperatures lower than  $10^5 \text{ K}$  certainly tells something about the heating/cooling processes within prominences. Moreover, helical and rotational motions have been detected (Liggett and Zirin 1984, Vrsnak 1990, Schmieder et al. 1998, these proceedings). Perhaps, prominence fine structures are more unstable than commonly believed as evidenced by “impulsive brightenings/velocity transients” seen in  $H\alpha$  by Toot and Malville (1987).

In activated prominences (Disparation brusques, etc.) which lead to Coronal Mass Ejections, one finds very high values (larger than the liberation speed). In the diagnostic lines, the Doppler dimming/brightening effect (e.g., in  $H\alpha$ , Rompolt 1969) should not be forgotten.

## 2.6. Oscillations

Oscillations are better (and more surely) detected in velocities (Balthasar and Wiehr 1994, Molowny-Horas et al. 1997). The last authors distinguish three cat-

egories of periods: short ( $< 5$  min); intermediate (6–20 min); and long (40–90 min) periods.  $H\beta$  measurements indicate a strong power at 7.5 min, a propagation over less than 20,000 km, and a lifetime of about 12 min. These results raise the issue of Alfvén waves and their role in heating, an idea also proposed by Yi and Engvold (1992). Measurements also point at the coupling of the prominence with the chromosphere and the corona. Energy inputs can be studied via intensity and velocities fluctuations.

### 3. Optically Thick Lines and Modelling

Diagnostics with optically thick lines are complex and involve the most plasma parameters (densities, temperature, filling factors, etc.). It is nevertheless necessary, even for optically thin lines which are influenced by optically thick lines in the atom (ion) system. Since the pioneering works by Heasley, Mihalas, Milkey, Morozhenko, Poland, Yakovkin, improved computations with “true” (OSO8) incident radiation profiles and PRD (Heinzel, Gouttebroze and Vial 1987) have been made. No match was found for the computed ratio  $L\alpha/L\beta$ , still higher than the observed one (the problem is more severe than in the chromosphere).

GHV initiated the construction of a wide set of empirical models, with the triple objective of: 1) Predicting observable lines, deriving physical quantities from observed spectra, and finding to what physical parameters lines are sensitive; 2) Drawing some laws that may help to understand what physical processes are at work; and 3) Providing benchmarks for the validation of more sophisticated models, e.g., two-dimensional codes (Paletou 1995). GHV prominence models consist of isothermal, isobaric slabs standing vertically above the solar surface. The hydrogen atom model consists of twenty levels and the continuum. 140 panels corresponding to the 140 models have been produced (see GHV). Correlation plots have been obtained by HGV, e.g.,  $H\alpha$  vs.  $H\beta$  and  $H\alpha$  vs. Emission Measure ( $n_e^2 D$ ) (Figure 2).

Coupling the last correlation plot with an independent measurement of the electron density,  $n_e$ , leads to the determination of the (effective) thickness,  $D$ , of the structure (Heinzel et al. 1996): 100 to 30,000 km (Figure 3). However, these values are in contradiction with Kippenhahn-Schlüter (KS) models derived from the same set of measurements (Heinzel and Anzer 1998, these proceedings). KS models have smaller thicknesses and higher pressures.

Other relations obtained by GHV and HGV include: Lyman continuum vs. column mass,  $T_{color}$  of the Lyman continuum vs.  $T_e$ ,  $L\alpha$  vs. pressure,  $L\alpha/L\beta$  vs. pressure,  $n_e^2$  vs.  $n_2$ , etc. Similar computations have been performed in Ca II by Gouttebroze et al. (1997 GVH). GVH computed exactly the ionization of Ca I and Ca II for different temperature and pressure models. Correlations between Ca II lines and Ca II/hydrogen lines have been obtained. Figure 4 shows K (3933Å) and infrared (8542Å) Ca II profiles for various conditions.

Let's mention the technique of the cloud models which Mein et al. (1996) improved noticeably, since it is now possible to take into account a varying  $H\alpha$  source function and velocity gradients within the filament. This fast technique is efficient for deriving velocity fields from MSDP data.

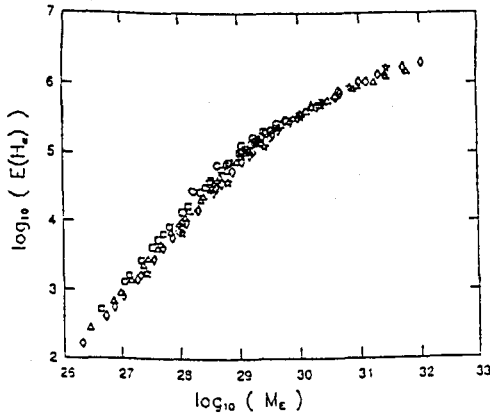


Figure 2. Correlation plot between Ha intensity and Emission Measure obtained from the set of 140 models of GHV. (From HGV).

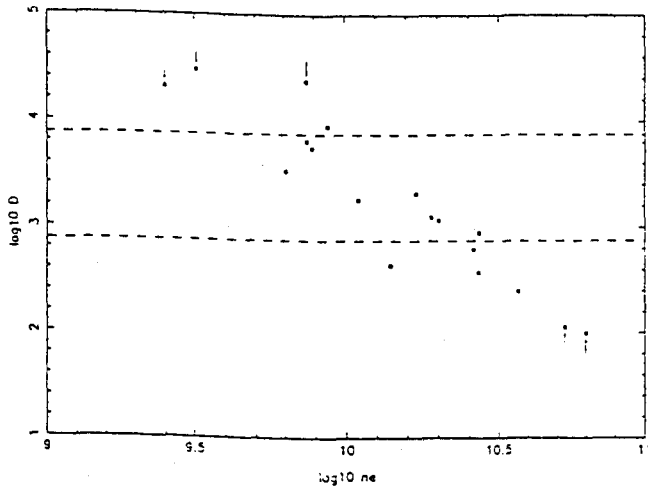


Figure 3. Geometrical thickness (in km) versus electron density for the set of prominences studied by Bommier et al. (1994). The two dashed lines show the thickness of 1 and 10 arcsec, respectively. (From Heinzel et al. 1996).

### 3.1. Effect of Radial Velocities

The above mentioned NLTE techniques must be modified in order to take into account the Doppler dimming/brightening in a moving atmosphere. The first non-LTE and transfer computations were performed by Heinzel and Rompolt (1987). More recently, modelling with Partial Frequency Redistribution (PRD) has been done by Gontikakis et al. (GVG1 and GVG2 1997). Basic results are as follows:

Taking account of PRD leads to higher  $L\alpha$ ,  $L\beta$ , and even  $H\alpha$  intensities and intensified ionization. The coherent scattering produced by PRD gives lines asymmetries, especially in the  $L\alpha$  line (Figure 5). One notices line profiles and

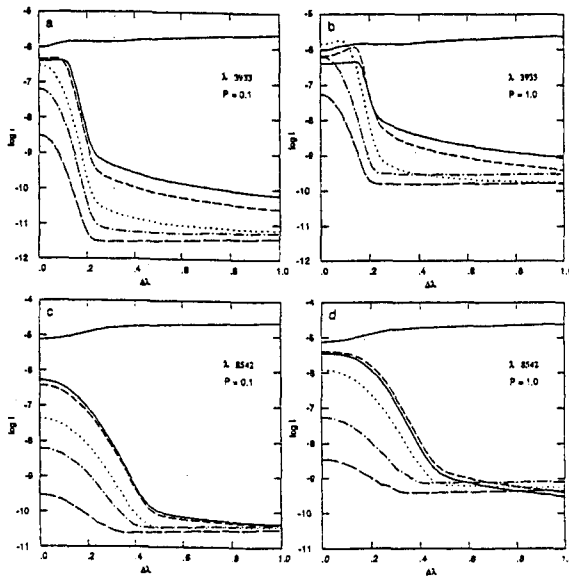


Figure 4. Ca II line half-profiles emitted by prominence models for different temperatures and pressures. The flat upper curve represents the intensity at disk center, for comparison. For the other curves, the solid line corresponds to 4300K, short dashes to 6000K, dots to 8000K, dot-dashes to 10,000K, long dashes to 15,000K. Panel (a): K line,  $P = 0.1 \text{ dyn cm}^{-2}$ . (b): K line,  $P = 1 \text{ dyn cm}^{-2}$ . (c): 8542Å,  $P = 0.1 \text{ dyn cm}^{-2}$ . (d): 8542Å,  $P = 1 \text{ dyn cm}^{-2}$ . (From GVH)

intensity variations with the thickness of the layer. The correlation between  $H\alpha$  and Emission Measure is also modified. A diagnostic of eruptive prominences is now possible, including the determination of the true velocity vector,  $V$ .

#### 4. Magnetic Field

As summarized by Leroy (1989) and updated by Bommier et al. (1994), the magnetic field has different properties in quiescent and active prominences.

In quiescent prominences, the field is horizontal and has a large shear angle,  $\alpha$  (the angle between the field and the filament is about  $25^\circ$ ) (see Figure 6). As confirmed by Bommier and Leroy (1998, these proceedings), they mostly have an inverse configuration. The field strength seems to increase with height, but the field is homogeneous and slowly varying. Its magnitude is in the range 3–30 G. ETH suggests an average value of 8 G. Because of the large range of gaseous (see above) and magnetic pressures, the plasma  $\beta$  may vary from about 0.001 to 3. The ambiguity in the direction has been solved using different techniques (see Leroy 1989). In active region prominences, the average field is in the range 20 to 70 G according to ETH. The magnetic configuration is mostly normal.

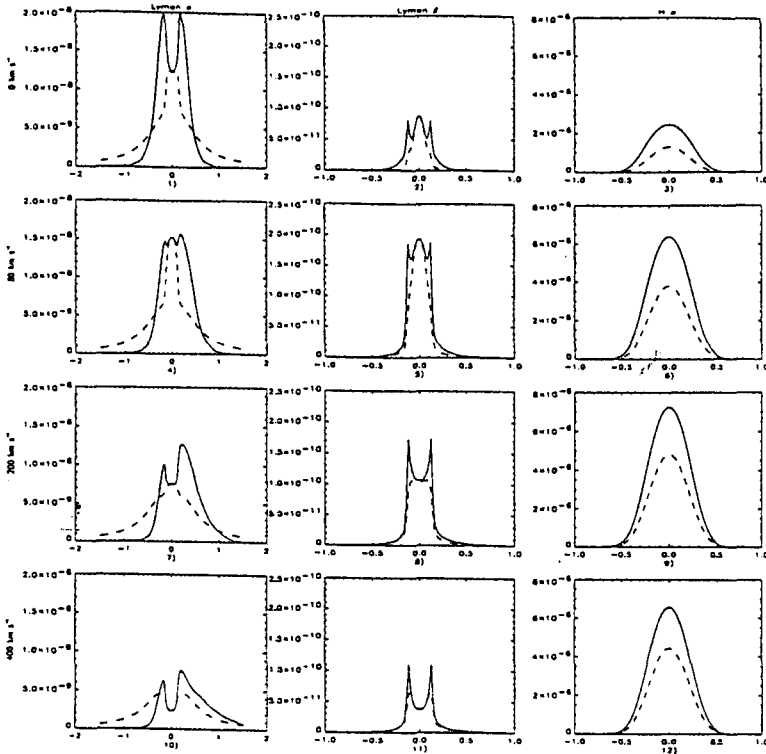


Figure 5. The profiles of  $L\alpha$ ,  $L\beta$  and  $H\alpha$  (columns 1, 2, 3) for four velocities: 0, 80, 200 and 400 km/s (rows 1, 2, 3 and 4). The model has a temperature of 8000K, a thickness of 2000 km and a pressure of  $0.1 \text{ dyn cm}^{-2}$ . PRD corresponds to the solid line and CRD to the dashed line. The intensity is in  $\text{ergs}^{-1} \text{cm}^{-2} \text{sr}^{-1} \text{Hz}^{-1}$  and the abscissa is in  $\text{\AA}$ .

#### 4.1. Electric field

Stark-polarized line profiles of hydrogen Paschen lines 18–3 allow us to detect electric fields perpendicular to the line-of-sight (Casini and Foukal 1996). Nine bright prominences have been observed by Foukal and Behr (1995) who found that 5 V/cm is an upper limit for the electric field. These authors raise the issue of the validity of KR model for low latitude prominences.

### 5. Prominence Fine Structure

There is direct evidence of small-scales in intensity and velocity images (Heinzel and Vial 1992), such as the vertical threads in Dunn's movie along which the material flows. Such evidence questions the compatibility between small-scale downflows and uniform horizontal magnetic field. This may be the indication that the core of small structures is dense and not very ionized. There are many indirect evidences of small-scale structure. For instance, Engvold et al. (1980)

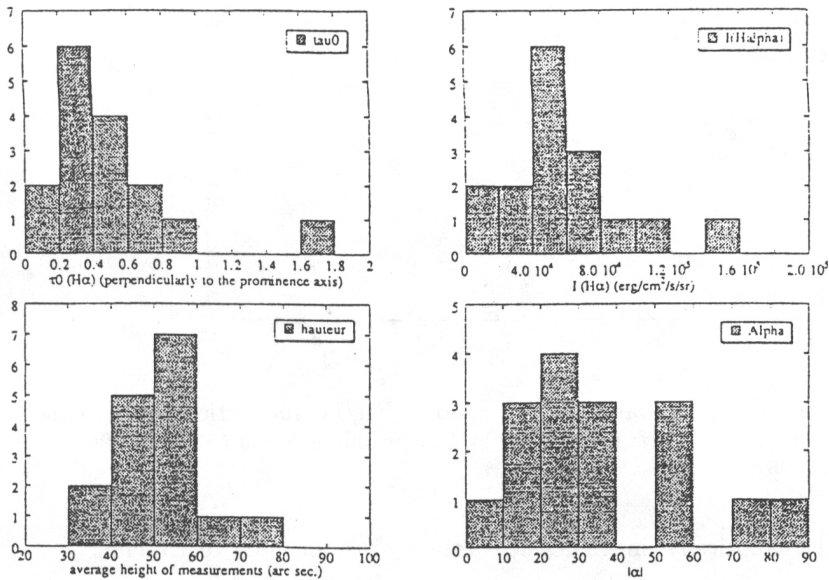


Figure 6. Histogram of  $\tau_{0}$  (optical thickness in  $H\alpha$ ),  $I(H\alpha)$  (measured intensity in  $H\alpha$ ), hauteur (height of observations, in arcsec) and Alpha (angle between the field vector and the prominence long axis). From Bommier et al. 1994.

studied the influence of the spatial resolution on line broadening,  $\langle v \rangle$ , and line shift,  $v$ : they found that  $\langle v \rangle$  decreases and  $v$  increases with better spatial resolution.

There also is much information in the distributions of  $H\alpha$  intensities, line shifts and widths, as measured on the disk (Mein and Mein 1991) or at the limb (Zirker and Koutchmy 1991). The presence of about 10 to 20 structures along the line of sight have been derived. According to Mein (1994), this is a lower limit since one should distinguish three characteristic lengths:  $L_T$  (characteristic of temperature and density fluctuations),  $L_V$  (velocities) and  $L_B$  (magnetic field) with  $L_T < L_V < L_B$ . This means that one may have clusters of threads with the same velocities or magnetic field. Poland and Tandberg-Hanssen (1983) and Cheng (1980) found evidence of different threads at different temperatures at medium scales. Small filling factors (0.01–0.1) have been found in the PCTR which imply that the density in these threads may be two orders of magnitude larger than the “average” density.

At high spatial and temporal resolution, we have a “chaotic picture” (Jensen 1990). The problem of support is now the one of supporting material on individual tubes of force on very short time-scales (minutes). A possible candidate has been advanced by Jensen (1990): Alfvén waves, generated in the convective zone, become non-linear and are trapped in prominences; in the dissipation process, momentum is transferred from waves to material. In the area of fine

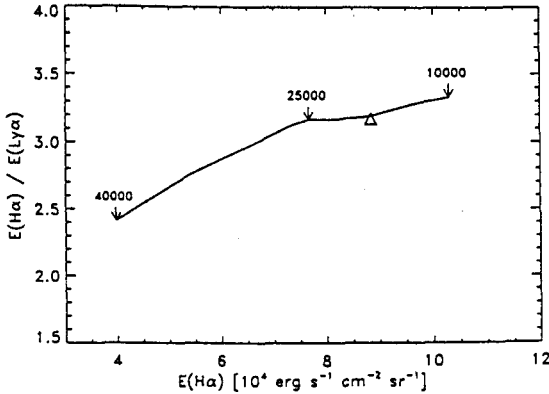


Figure 7. Variation of the ratio of  $H\alpha/L\alpha$  intensities with  $H\alpha$  intensity at different altitudes in the prominence slab. From Paletou (1996).

structure, optically thick lines have recently proven to be very useful.

### 5.1. Optically Thick Threads and Modelling

- a. In the two-dimensional modelling of Paletou, not only two-dimensional effects are taken into account (from the point of view of illumination and photon escape), but the filament emission can be properly computed and the backscattered radiation of the filament towards the chromosphere included (Paletou 1995). Figure 7 shows the variation of the ratio  $H\alpha/L\alpha$  with the  $H\alpha$  emission along the filament height (Paletou 1996). Paletou (1998, these proceedings) also addressed the issue of the visibility of bright rims (“marges”); he found no major increased excitation at the bottom of the filament/slab, contrary to Heinzel et al. (1995).
- b. In the multi-thread modelling of Fontenla et al. (FRVG 1996), the thread (replaced by a slab) is defined by the balance between radiative losses and conduction and is constructed from a fixed central temperature to a coronal temperature. FRVG take into account the PRD and the ambipolar diffusion but no radiative interaction between threads (see Heinzel 1989). The ionization degree (ID) is never less than 2.5. The radiative losses increase by more than an order of magnitude below  $10^5\text{K}$ , as compared with Cox and Tucker. FRVG computed the variations of lines profiles with the pressure and the number of threads. They need about 100 threads to match the  $L\alpha$ ,  $L\beta$  and  $H\alpha$  intensities and profiles (Figure 8). The  $L\alpha/L\beta$  ratio is closer to the observed one, but agreement with observations is only obtained with a cool core in the model.
- c. Other techniques take into account randomly distributed inhomogeneities (e.g., Nikoghossian et al. 1997).

## 6. Prospects

We anticipate progress on the following issues:

1. Better measurements of the magnetic field in prominences and better connec-

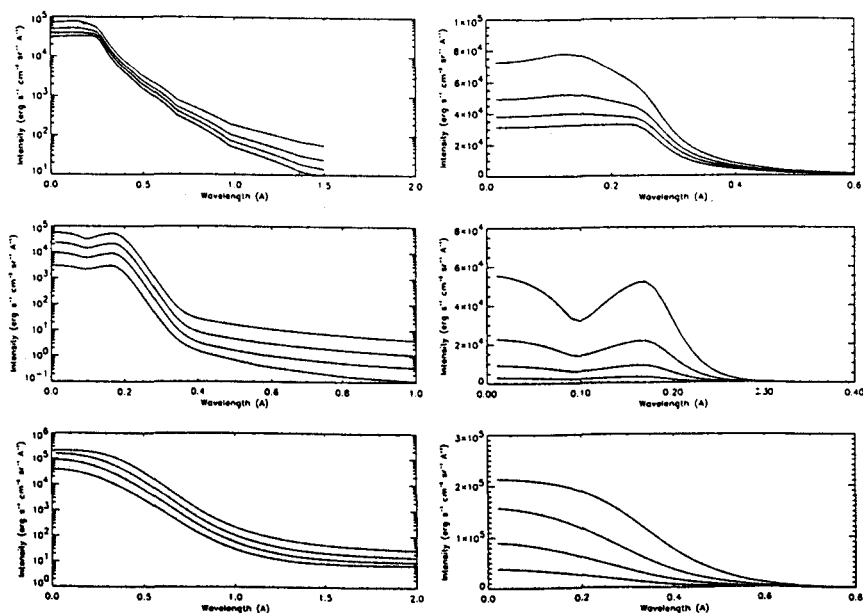


Figure 8. Computed half-profiles of  $L\alpha$  (first row),  $L\beta$  (second row), and  $H\alpha$  (third row) for four different pressures. The first column is a semi-log plot to better see the far wing; the second column is a linear plot. (From FRVG 1996).

tion with the photospheric magnetic structure, a major task to which THEMIS is devoted. One can also expect major progress in field extrapolation. One could say that prominences are the testbed of all techniques of field extrapolations.

2. Better spectroscopic diagnostics: SOHO provides increased temperature coverage, good time resolution, and continuous observing sequences. The IR (1.6  $\mu$ m, continuum, He) may prove to be very useful for detecting the lowest temperatures (Hirayama et al. 1979).

3. When possible, *simultaneous* spectroscopic and magnetic measurements that can provide the  $\beta$  of the plasma.

4. Modelling: studies should include non-LTE transfer combining a multilevel atom, partial frequency redistribution *and* realistic geometries. They should be done in as many lines and continua from different atoms and ions as possible.

5. Energy and mass budget (magnitude and location): detailed radiation budgets (with lines spanning temperatures of  $10^4 - 10^8$  K) are possible with SOHO.

6. Oscillations: their measurements in different lines provide information on the connection of the prominence and its environment. We may well be *en route* towards prominence seismology.

7. Fine structure: If one wants to have direct evidence, what are the required spatial and temporal resolutions? If one relies on indirect evidence (measurements of filling factors), how reliable is the density diagnostic? What is the impact of flows on the departure from ionization equilibria?

**References**

- Balthasar, H. and Wiehr, E. 1994, *A&A*, 286, 639
- Bastian, T.S., Ewell, M.W. Jr. and Zirin, H. 1993, *ApJ*, 418, 510
- Bommier, V., Leroy, J.L., Sahal-Brechot, S. 1986, *A&A*, 156, 79
- Bommier, V. et al. 1994, *Sol. Phys.*, 154, 231
- Casini, R. and Foukal, P. 1996, *Sol. Phys.*, 163, 65
- Cheng, C.-C. 1980, *Solar Phys.*, 65, 347
- Chiuderi, C., and Chiuderi-Drago, F. 1991, *Sol. Phys.*, 132, 81
- Chiuderi-Drago, F., Engvold, O. and Jensen, E. 1992, *Sol. Phys.*, 139, 47
- Engvold, O., Wiehr, E. and Wittmann, A. 1980, *A&A*, 85, 326
- Engvold, O. 1989, in *Dynamics and Structure of Quiescent Solar Prominences*, (ed.) E.R. Priest, Kluwer Acad. Publ., Dordrecht, Holland, p. 47
- Engvold, O. et al. 1990, in *Dynamics of Quiescent Prominence*, Ruzdjak, V. and Tandberg-Hanssen, E. (eds.), Springer-Verlag, New York, p. 294
- Fontenla, J., Rovira, M., Vial, J.-C. and Gouttebroze, P. 1996, *ApJ*, 466, 496
- Foukal, P., Hoygt, C., and Gilliam, L. 1986, *ApJ*, 303, 86
- Foukal, P. and Behr, B. B. 1995, *Sol. Phys.*, 156, 293
- Gontikakis, C., Vial, J. and Gouttebroze, P. 1997, *Sol. Phys.*, 172, 189 (GVG1)
- Gontikakis, C., Vial, J. and Gouttebroze, P. 1997, *A&A*, 325, 803 (GVG2)
- Gouttebroze, P., Heinzel, P. and Vial, J.-C. 1993, *A&AS*, 99, 513
- Gouttebroze, P., Vial, J.-C., and Heinzel, P. 1997, *Solar Phys.*, 172, 125
- Harrison, R.A. et al. 1993, *A&A*, 274, L12
- Heasley, J.N. and Milkey, R.W., 1983, *ApJ*, 268, 398
- Heinzel, P. and Rompolt, B. 1987, *Solar Phys.*, 110, 171
- Heinzel P., Gouttebroze P. and Vial J.-C. 1987, *A&A*, 183, 351
- Heinzel, P. 1989, *Hvar Observatory Bull.*, 13, p. 317
- Heinzel, P. and Vial, J.-C. 1992, in *Proc. of ESA Workshop on Solar Physics and Astrophysics at Interferometry Resolution*, ESA SP-348, p. 57
- Heinzel P., Gouttebroze P. and Vial J.-C. 1994, *A&A*, 292, 656
- Heinzel P., Kotrc, P., Mouradian, Z. and Buyukliev, G. 1995, *Sol. Phys.*, 160, 19
- Heinzel P., Bommier V. and Vial J.-C. 1996, *Solar Phys.*, 164, 211
- Hirayama, T., Nakagomi, Y. and Okamoto, T., 1979, in *Physics of Solar Prominences*, (eds.) E. Jensen, P. Maltby, and F.Q. Orrall, Oslo, p. 48
- Hirayama, T. 1990, in *Dynamics of Quiescent Prominences*, Ruzdjak, V. and Tandberg-Hanssen, E. (eds.), Springer-Verlag, New York, p. 187
- Jensen, E. 1990, in *Dynamics of Quiescent Prominences*, Ruzdjak, V. and Tandberg-Hanssen, E. (eds.), Springer-Verlag, New York, p. 129
- Landman, D.A. 1983, *ApJ*, 269, 728
- Landman, D.A. 1984, *ApJ*, 279, 438
- Landman, D.A. 1985, *ApJ*, 290, 369

- Landman, D.A. 1986, *Ap.J.*, 305, 546
- Leroy, J.-L. 1989, in *Dynamics and Structure of Quiescent Prominences*, (ed.) E.R. Priest, Kluwer Acad. Publ., Dordrecht, Holland, p. 77
- Liggett, M. and Zirin, H. 1984, *Solar Phys.*, 91, 259
- Mein, P. and Mein, N. 1991, *Solar Phys.*, 136, 317
- Mein, P. 1994, in *Solar Coronal Structures*, (eds.) V. Rusin, P. Heinzel and J.-C. Vial, Tatranska Lomnica, Slovakia, p. 289
- Mein, N. et al. 1996, *A&A*, 275, 283
- Molowny-Horas, R. et al. 1997, *Solar Phys.*, 172, 181
- Nikoghossian, A.G., Pojoga, S. and Mouradian, Z. 1997, *Solar Phys.*, 325, 813
- Paletou, F. 1995, *A&A*, 302, 587
- Paletou, F. 1996, *A&A*, 311, 708
- Poland, A.I et al. 1971, *Solar Phys.*, 18, 391
- Poland, A.I. and Tandberg-Hanssen, E. 1983, *Solar Phys.*, 84, 63
- Rabin, D. 1986, in *Coronal Prominence Plasmas*, NASA CP-2442, A. Poland (ed.), p. 135
- Rompolt, B. 1969, *Acta Universitatis Wratislaviensis*, 77, 117
- Schmahl, E.J. and Orrall, E.Q. 1979, *ApJ*, 231, L41
- Schmahl, E.J. and Orrall, E.Q. 1986, in *Coronal Prominence Plasmas*, NASA CP-2442, A. Poland (ed.), p. 127
- Schmieder, B. 1990, in *Dynamics of Quiescent Prominences*, Ruzdjak, V. and Tandberg-Hanssen, E. (eds.), Springer-Verlag, New York, p. 85
- Simon, G., Schmieder, B., Démoulin, P. and Poland, A.I. 1986, *A&A*, 166, 319
- Stellmacher, G. and Wiehr, E. 1997, *A&A*, 319, 669
- Stellmacher, G., Koutchmy, S. and Lebecq, C. 1986, *A&A*, 167, 351
- Tandberg-Hanssen, E. 1995, *The Nature of Solar Prominences*, Kluwer Academic Press, Dordrecht, Holland
- Toot, G.D. and Malville, J.M. 1987, *Solar Phys.*, 112, 67
- Vial, J.-C. 1982, *Ap.J.*, 254, 780
- Vrsnak, B. 1990, *Sol. Phys.*, 129, 295
- Wiik, J.-E., Schmieder, B. and Noens, J.C. 1992, *Solar Phys.*, 149, 51
- Wiik, J.-E., Dere, K.P. and Schmieder, B. 1993, *A&A*, 273, 267
- Yi, Z. and Engvold, O. 1992, *Sol. Phys.*, 134, 235
- Zirker, J.B. and Koutchmy, S. 1991, *Solar Phys.*, 131, 107